IEEE Access
Multidisciplinary | Rapid Review | Open Access Journal

Received April 1, 2019, accepted April 11, 2019, date of current version May 1, 2019.

Digital Object Identifier 10.1109/ACCESS.2019.2912067

Collision Avoidance/Mitigation System: Motion Planning of Autonomous Vehicle via Predictive Occupancy Map

KIBEOM LEE AND DONGSUK KUM, (Member, IEEE)
Graduate School of Green Transportation, Korea Advanced Institute of Science and Technology (KAIST), Daejeon 34141, South Korea

Corresponding author: Dongsuk Kum (dskum@kaist.ac.kr)

This work was supported by the Development of Deep Learning-Based Future Prediction and Risk Assessment Technology considering Inter-vehicular Interaction in Cut-in Scenario through the Technology Innovation Program funded by the Ministry of Trade, Industry, and Energy, South Korea, under Grant 10083646.

ABSTRACT Despite development efforts toward autonomous vehicle technologies, the number of collisions and driver interventions of autonomous vehicles tested in California seems to be reaching a plateau. One of the main reasons for this is the lack of defensive driving functionality; i.e. emergency collision avoidance when other human drivers make mistakes. In this paper, a collision avoidance/mitigation system (CAMS) is proposed to rapidly evaluate risks associated with all surrounding vehicles and to maneuver the vehicle into a safer region when faced with critically dangerous situations. First, a risk assessment module, namely, predictive occupancy map (POM), is proposed to compute potential risks associated with surrounding vehicles based on relative position, velocity, and acceleration. Then, the safest trajectory with the lowest risk level is selected among the 12 local trajectories through the POM. To ensure stable and successful collision avoidance of the ego-vehicle, the lateral and longitudinal acceleration profiles are planned while considering the vehicle stability limit. The performance of the proposed algorithm is validated based on side and rear-end collision scenarios, which are difficult to predict and to monitor. The simulation results show that the proposed CAMS via POM detect a collision risk 1.4 s before the crash, and avoids the collision successfully.

INDEX TERMS Autonomous vehicle, advanced driver assist system (ADAS), collision avoidance, risk assessment, motion planning.

I. INTRODUCTION

Autonomous vehicles have been one of the most active research topics in an automotive industry hoping to maximize safety and user convenience. In terms of safety, many researchers argue that autonomous vehicle technologies will substantially reduce the number of collisions, because 90% of collisions are caused by human error [1]. Although automated and autonomous vehicles will eliminate simple human errors such as those resulting from texting and drowsiness, automated vehicles will lead to other collisions that human drivers would have been able to avoid, e.g. through defensive driving [2], [3]. For instance, Waymo's autonomous vehicles (a.k.a. Google cars) often experience collisions caused by other vehicles at fault [2], [3]. In a September 2016 accident, Waymo's autonomous vehicle was hit by a van running a red light at an intersection in California. In another case, the Waymo van in autonomous mode collided with an onrushing vehicle that drove over the centerline in Arizona in May 2018. In these scenarios, if human drivers had been driving the vehicles, collisions would not have occurred as drivers would have made defensive maneuvers. Unfortunately, the most advanced autonomous vehicles today, such as Google cars, still cannot make such decisions to avoid collisions initiated by other vehicles [3]. In fact, many prior autonomous vehicle technologies focused on improving intelligence of risk predictions and path planning during normal conditions. In order to resolve these limitations, a collision avoidance/

The associate editor coordinating the review of this manuscript and approving it for publication was Zheng Chen.

2169-3536 © 2019 IEEE. Translations and content mining are permitted for academic research only.
Personal use is also permitted, but republication/redistribution requires IEEE permission.
See http://www.ieee.org/publications_standards/publications/rights/index.html for more information.

mitigation system (CAMS) is proposed, in which the CAMS can override the normal driving algorithm when a collision is imminent.

In the literature, in order to avoid collisions from unexpectedly approaching vehicles, many researchers plan collision avoidance trajectories by focusing on single obstacles. When a target obstacle is detected, the system plans the path to avoid the obstacle based on the location and size of the obstacle [4]. Guo *et al.* proposed a steering and braking control algorithm for vision-based emergency obstacle avoidance [5]. Isermann *et al.* proposed a tracking method that developed a velocity profile based on optimal trajectory and obstacle size and position [6]. Hesse and Sattel based on potential field and elastic band theory, developed a path and velocity profile that avoids obstacles at the front of the vehicle while reaching target position [7]. However, in actual collision avoidance situations, considering one obstacle is very limited.

When a vehicle steers to avoid an obstacle, it will go out of its current lane. Thus, it is essential to check all surroundings of the ego vehicle and ensure that the planned trajectory is safe for the vehicle to follow. Otherwise, when avoiding target obstacles, vehicle will collide with other nearby obstacles. To resolve such limitations, there have been studies that have considered all risks of the vehicle surrounding environment based on the potential field [8]–[12]. Kim *et al.* proposed a method using a potential risk concept that identifies potential risk of surroundings and finds the safest optimal path [13]. The multi-vehicle problem may have been resolved, but the risk to the surrounding vehicles is determined based on the current position. However, since surrounding vehicles are moving fast, it is dangerous to plan collision avoidance paths based on current position. For safe collision avoidance, it is necessary to predict trajectories of surrounding vehicles.

In vehicle research groups, trajectory prediction algorithms have been studied [14]–[16]. However, it is difficult to use these advanced algorithms to derive predictions results quickly in situations of impending collision. The physics based motion model can produce sufficiently high prediction accuracy 1 to 2 seconds before the moment of collision [17]–[21]. This method is also well suited for collision avoidance algorithms with fast computation speeds. The trajectory prediction result is described as vehicle's future position or time-series OGM. However, these results do not indicate the risk to surrounding vehicles.

Based on the trajectory prediction results, a risk assessment algorithm is needed. Risk assessment determines the danger of trajectories planned for the ego vehicle based on future prediction. The most commonly used risk indicator is time-to-collision (TTC), which will predict the time at which the ego vehicle will collide with an obstacle [22]–[24]. To overcome the limitations in using deterministic properties for the risk indicator, probability-based collision probabilistic methods have been researched as well [25]–[28]. However, the risk index can only be determined under the condition that ego-vehicle and target vehicle paths are known. Furthermore, the risk index is suitable for two-vehicle collisions, but cannot be applied in multi-vehicle collision situations [29]. For collision avoidance maneuvers, a multi-vehicle risk assessment algorithm in necessary.

In this paper, a collision avoidance/mitigation algorithm has been proposed that is based on POM. The risk of each candidate trajectory can be evaluated and selected quickly in multi-vehicle situations using POM, which represents the risk for each space based on the predicted surrounding vehicle trajectories. This algorithm can overcome the limitations mentioned from previous studies and safely mitigate the potential risks caused by sudden maneuvers of surrounding vehicles. The main ideas proposed in this paper is 1) the Predictive Occupancy Map (POM), which can simultaneously identify potential risks in spatial and temporal space. POM is able to solve the problem of all-around risk assessment and multi-vehicle risk assessment based on future trajectory prediction results. 2) A trajectory risk assessment algorithm that determines the risks of trajectories selected through the POM. An omnidirectional pre-determined trajectory can be compared fairly based only on the surrounding risk. 3) A local motion planning algorithm that generates an acceleration profile while simultaneously considering trajectory and velocity.

The remainder of this paper is organized as follows: In Section II, an overview of the proposed collision avoidance/mitigation system and algorithm is provided. In section III, a predictive occupancy map design method is proposed. In section IV, a trajectory candidate risk assessment based on POM and motion planning study is carried out. In section V, an algorithm is investigated using simulation with representative collision scenarios. Finally, Section VI provides the concluding remarks.

II. PROPOSED COLLISION AVOIDANCE/ MITIGATION SYSTEM

In this section, the operating concept of the proposed collision avoidance/mitigation system (CAMS) is discussed. The activation conditions, based on ego vehicle collision risk and sequence of CAMS algorithm, are described.

A. ACTIVATION OF COLLISION AVOIDANCE/ MITIGATION SYSTEM

Previous algorithms were developed with a focus on reducing errors caused by the ego vehicle. CAMS estimates the future based on the surroundings of the ego vehicle and determines its collision risk accordingly. Figure 1 illustrates the proposed drive mode decision process of the autonomous vehicle. The vehicle will constantly monitor its surroundings and, if ego vehicle collision risk (Risk_{ego}) exceeds a pre-determined threshold ($\text{Risk}_{\text{threshold}}$), the Collision avoidance/mitigation algorithm will override the currently active algorithm and will plan the vehicle's future trajectory and track accordingly. Once CAMS is executed it will remain active for a certain period, which is described as follows

$$\text{t}_{\text{CAMS}} = k \cdot \Delta t \quad (t_0 \leq \text{t}_{\text{CAMS}} < t_f) \tag{1}$$

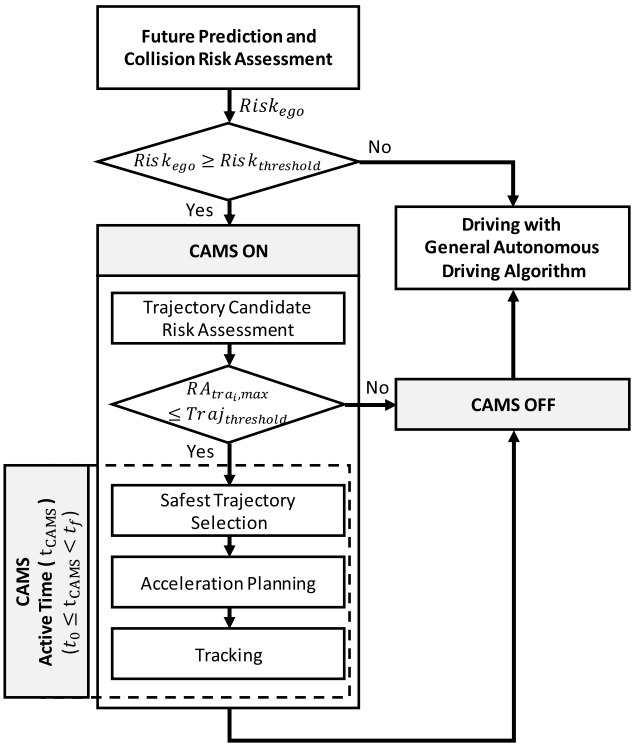

FIGURE 1. Flow chart of driving mode (general autonomous driving mode and collision avoidance/mitigation driving mode) decision process.

where t_{CAMS} is the collision avoidance/mitigation system active time, t_0 is the collision avoidance/mitigation system start time, t_f is the collision avoidance/mitigation system final time, k is the iteration number, and Δt is the time interval of each step.

When t_{CAMS} reaches t_f, the CAMS terminates, and then the general autonomous driving algorithm executes driving again. When CAMS is on, but there is no safe trajectory because the risks of all trajectories are larger than the trajectory risk threshold ($Traj_{threshold}$), it indicates that the current driving space is a relatively safe space. In this case, the vehicle drives with a general autonomous driving algorithm and waits for a safe avoidance space to evade collision.

This study does not focus on sensing technology; it is assumed that accurate information of ego vehicle surroundings is sent as input. Future prediction and risk assessment of the proposed algorithm is conducted in areas where sensing is available, and areas that are not sensed are ignored.

B. OVERVIEW OF COLLISION AVOIDANCE/ MITIGATION ALGORITHM

Figure 2 shows the overall control architecture of the proposed collision avoidance/mitigation system. CAMS algorithm operates, in order, starting with prediction, risk assessment, and motion planning. Prediction of future vehicle position is conducted with the constant acceleration (CA) model. There are various prediction models that have already been developed. However, in unexpected situations close to collision, there are not enough data to predict vehicle behavior and method provides inaccurate results. The CA model can provide accurate prediction within a short term of 2 seconds, and is suitable for vehicle future prediction in unexpected situations.

Much research on risk assessment algorithms has been conducted. However, risk has been assessed with a focus on a single vehicle, and risks for pedestrian, other vehicles, and surrounding environment were done separately. To overcome this problem, this study proposes a POM that can integrate all the surrounding risks, including time and space information. Through the risk assessment stage, the risk of the ego vehicle ($Risk_{ego}$) and a risk map of its surroundings are calculated.

When the vehicle is involved in an emergency in which it nearly reaches vehicle friction/stability limit, the trajectory and velocity must be simultaneously planned; as well, it is necessary to determine that the planned route is physically viable for vehicle to drive. In the motion planning section of the proposed method, the route and vehicle velocity can be simultaneously considered through the g-g diagram and local trajectory candidate. The CAMS is activated when the longitudinal velocity is set above 5m/s due to vehicle's non-holonomic dynamic characteristics. The system will be deactivated at velocity under 5m/s.

III. PREDICTIVE OCCUPANCY MAP (POM)

In this section, the design procedure allowing the POM to observe the surrounding risks is discussed. When vehicle is operating on a freeway, 'dangerous' objects are categorized into two parts: surrounding vehicles and the driving environment. Surrounding vehicles consist of obstacles near the road, static vehicles, and dynamic vehicles, while driving environment consists of drivable regions and traffic lanes.

Setting the ego vehicle as the base coordinate, and determining surrounding vehicles and their relative positions, velocity, and acceleration, the POM can predict future positions with respect to time. The POM will designate the most dangerous space and least dangerous space with ratings of 5 and 0, respectively. To achieve exact risk assessment and provide the most suitable trajectory for vehicle to drive, the ego vehicle's driving information is needed; it can be acquired through sensors equipped on the vehicle as shown below

$$X_{ego} = [p_{ego,x}, p_{ego,y}, V_{ego,x}, V_{ego,y}, A_{ego,x}, A_{ego,y}] \quad (2)$$

where X_{ego} is the set of ego vehicle driving information, p_{ego} is the ego vehicle local position, V_{ego} is the ego vehicle velocity, A_{ego} is the ego vehicle acceleration, and subscripts x and y are the x-axis and y-axis, respectively. Since the coordinates are relative to the ego vehicle, the value of p_{ego} is zero.

A. RISK MAP GENERATION FOR SURROUNDING VEHICLES

When evaluating the level of risk for the vehicle, the position, velocity, and acceleration of the obstacle and the surrounding vehicles are assessed and its future position is predicted.

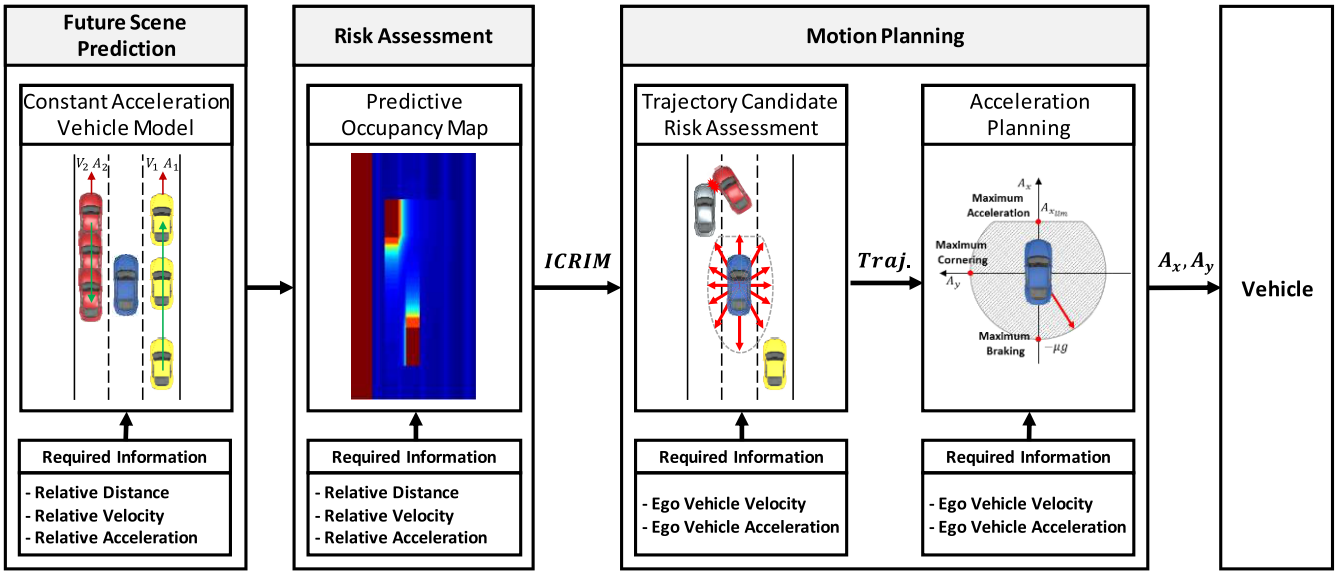

FIGURE 2. Collision avoidance/mitigation system architecture diagram.

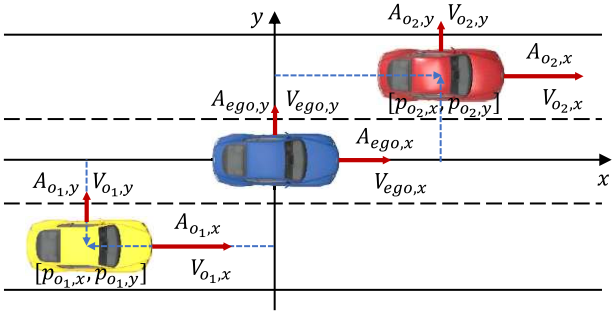

FIGURE 3. Ego vehicle fixed coordinates and surrounding vehicle information.

1) OCCUPANCY PREDICTION MODEL FOR SURROUNDING VEHICLES

To predict the future positions of surrounding vehicles, Fig. 3 shows the corresponding position, velocity, and acceleration of surrounding vehicles relative to the ego vehicle. The information for surrounding vehicles is expressed in Eq. (3), while the relative information between the ego vehicle and surrounding vehicles is expressed in Eq. (4)

$$X_{o_n} = [p_{o_n,x}, p_{o_n,y}, V_{o_n,x}, V_{o_n,y}, A_{o_n,x}, A_{o_n,y}] \quad for\ n \in [1, \cdots, Obstacle\ number] \tag{3}$$

$$X_{r_n} = X_{o_n} - X_{ego} = [p_{o_n,x}, p_{o_n,y}, V_{r_n,x}, V_{r_n,y}, A_{r_n,x}, A_{r_n,y}] \tag{4}$$

where X_o is the set of surrounding vehicle driving information, p_o is the surrounding vehicle relative position, V_o is the surrounding vehicle velocity, a_o is the surrounding vehicle acceleration, V_{ego} is the ego vehicle velocity, a_{ego} is the ego vehicle acceleration, X_r is the set of surrounding vehicle relative driving information, V_r is the surrounding vehicle relative velocity, A_r is the surrounding vehicle relative acceleration, subscripts x and y are the x-axis and y-axis, respectively, and subscript n is the obstacle index.

In this study, short term prediction is carried out in imminent collision situations using the CA prediction model. The CA model predicts vehicle's future position while assuming that the current vehicle's velocity and acceleration are maintained. Therefore, the CA model can provide accurate prediction results in a short period, which is appropriate in unexpected driving situations such as near-collisions. The equation of motion of the simple CA model is expressed as

$$\Delta D = \frac{1}{2} \cdot A_r \cdot \Delta t^2 + V_r \cdot \Delta t \tag{5}$$

where ΔD is the driving distance within time interval of each step.

In order to acquire time (t) to arrival at a certain position (D_{o_n}) through Eq. (5), the time-to-occupancy (TTO) can be calculated.

$$TTO_n(D_{o_n}) = \frac{-V_r - \sqrt{V_r^2 - 2 \cdot A_r \cdot D_{o_n}}}{A_r} \tag{6}$$

Under normal driving circumstances, the TTO can provide accurate short-term prediction. However, for sudden unexpected situations, acceleration/deceleration surge may occur and can degrade prediction performance. Therefore, in Eq. (7), the idea of Advanced Time-to-occupancy (ATTO) is proposed; similar to a PD controller, ATTO can separate and adjust the effectiveness of the acceleration.

$$\mathrm{ATTO}_n(D_{o_n}) = \frac{D_{o_n}}{V_r + d \cdot A_r} \tag{7}$$

where d is the gain of the relative acceleration effect.

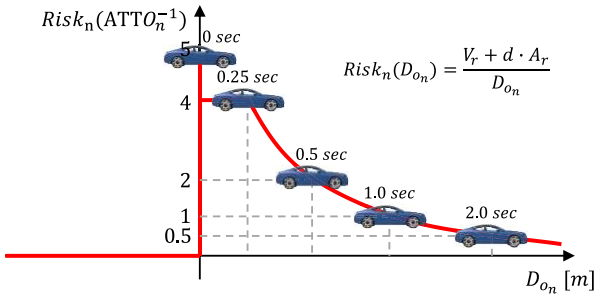

FIGURE 4. Example of single vehicle risk.

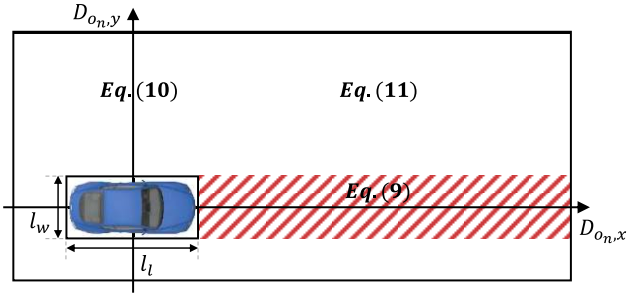

FIGURE 5. Two-dimensional collision risk assessment of surrounding vehicles.

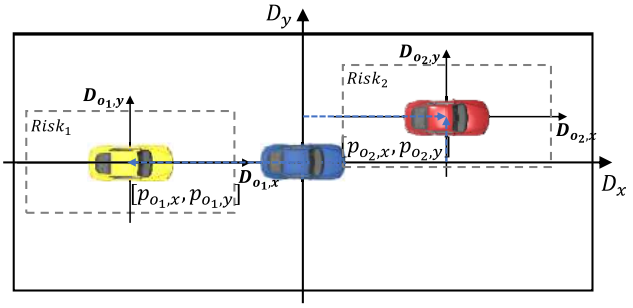

FIGURE 6. Placement of surrounding vehicle risk based on ego vehicle local coordinates.

2) RISK ASSESSMENT OF SURROUNDING VEHICLES

In transportation and vehicle research groups, the 'collision risk' has had various meanings, but the definition of risk has not been precisely defined. In this research, the ATTO is used as the risk. Using the ATTO based on the CA model proposed in the previous subsection, the arrival time of vehicles at specific positions can be predicted. In order to represent the risk by considering both current and future situations, it is necessary to define the risk by considering the concept of position relative to time. Therefore, the POM represents risk as a reciprocal of time taken for vehicle to be located at a certain point in space. This is expressed as '$Risk[D]$', and it also the inverse of ATTO, as shown below.

$$Risk_n(D_{o_n}) = ATTO_n^{-1}(D_{o_n}) \tag{8}$$

During ATTO $=$ 0 condition, when the vehicle collides, the ATTO^{-1} value becomes infinity. Therefore, the maximum risk ($Risk_{max}$) was set at 4 (ATTO $=$ 0.25 seconds). In addition, the current vehicle position was assigned a risk factor of 5, the highest risk value. In this case, the acceleration gain (d) is tuned with 0.1. Through Eq. (8), the risk for a single vehicle can be observed, as shown in Fig. 4.

Finally, the risk within two-dimensional space based on the center of an obstacle and surrounding vehicle considering vehicle size is given by Eq. (9) - (11) below and described in Fig. 5.

$$Risk_n(D_{o_n,x}, D_{o_n,y}) = \frac{V_{r,x} + d \cdot A_{r,x}}{D_{o_n,x} - l_l/2} \quad (|D_{o_n,y}| \le l_w/2) \tag{9}$$

$$Risk_n(D_{o_n,x}, D_{o_n,y}) = \frac{V_{r,y} + d \cdot A_{r,y}}{D_{o_n,y} - l_w/2} \quad (|D_{o_n,x}| \le l_l/2) \tag{10}$$

$$Risk_n(D_{o_n,x}, D_{o_n,y}) = \left(\frac{D_{o_n,x} - l_l/2}{V_{r,x} + d \cdot A_{r,x}} + \frac{D_{o_n,y} - l_w/2}{V_{r,y} + d \cdot A_{r,y}} \right)^{-1} \quad (|D_{o_n,x}| > l_l/2, |D_{o_n,y}| > l_w/2) \tag{11}$$

where l_l and l_w are the length and width of the vehicle, respectively, and subscripts x and y are the x-axis and y-axis, respectively.

3) INTEGRATION OF SURROUNDING VEHICLE RISK MAPS

By calculating the risk of all surrounding vehicles that are sensed around the ego vehicle, it is possible to integrate all surrounding risks. The risk of surrounding vehicles is determined relative to the position of the ego vehicle. The relative position of the surrounding vehicle risk is expressed as

$$Risk_{int_n}(D_x, D_y) = Risk_n(D_{o_n,x} - p_{o_n,x}, D_{o_n,y} - p_{o_n,y}) \tag{12}$$

After placing the risk of each obstacle relative to the position of the ego vehicle, the maximum risk values at each space are used to determine the overall risk ($Risk_{o\&v}$), which considers obstacles and surrounding vehicles. $Risk_{o\&v}$ is calculated using Eq. (13) and described in Fig. 6.

$$Risk_{o\&v} = sup(Risk_{int_1}, Risk_{int_2}, \cdots, Risk_{int_n}) \tag{13}$$

B. RISK MAP GENERATION FOR DRIVING ENVIRONMENT

Risks regarding driving environment are divided into two categories: drivable regions and traffic lanes. Similar to the risk considering surrounding obstacles and nearby vehicles, the driving environment design, which considers both drivable boundaries and risk involved from lane changes, is needed.

1) DRIVABLE REGION

The drivable region is determined to indicate the extent to which the vehicle can travel. In freeway conditions, the drivable region is determined based on barriers. Spaces inaccessible to vehicles were set at the highest risk value of 5. The equation of drivable region ($Risk_{bound}$) is expressed as

$$Risk_{bound} = 5\{step\left(D_y - B_l\right) + step\left(-D_y - B_r\right)\} \tag{14}$$

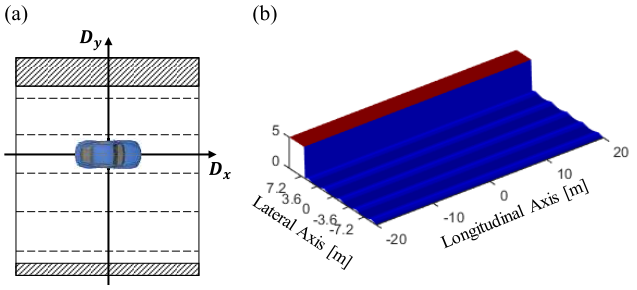

FIGURE 7. Concept of driving environment risk map.

where B_l and B_r are the distance of the left and right bounds to the vehicle center line, respectively; step means the step function.

2) TRAFFIC LANE

Changing the lane to avoid collision can alter the vehicle's driving traffic lane, and so can be relatively more dangerous than accelerating or decelerating the vehicle in the same lane. In addition, if the level of risk for traveling in the longitudinal direction or changing lanes to avoid collision are the same, longitudinal direction is preferred. To reflect these road conditions, traffic lane risk ($Risk_{lane}$) was formulated as

$$Risk_{lane} = -\left|lane_r \cdot \cos\left(\frac{\pi}{lane_w} \cdot D_y\right)\right| + lane_r \quad (15)$$

where $lane_r$ is the max risk value of lane, and $lane_w$ is the width of the traffic lane.

3) INTEGRATION OF DRIVABLE REGION AND TRAFFIC LANE RISKS

Traffic lane risk and drivable region risk are combined in driving environment risk ($Risk_{env}$), as shown in Eq. (16), while Fig. 7 shows the driving environment risk map based on the freeway. The closer the lane, the greater the risk by Eq. (15), and beyond the centerline, the risk indicate 5 by Eq. (14).

$$Risk_{env} = sup(Risk_{lane}, Risk_{bound}) \quad (16)$$

C. INTEGRATION OF SURROUNDING VEHICLES AND DRIVING ENVIRONMENT RISKS

The POM can be obtained by integrating the surrounding vehicle and driving environmental risks, as described in Eq. (17). Ego vehicle risk is expressed as the risk value at the (0, 0) point, which is the center of the vehicle in the POM.

$$POM = sup(Risk_{o\&v}, Risk_{env}) \quad (17)$$

D. SIMULATION RESULTS

The sample scenarios for the POM designed in the previous subsection are shown in Fig. 8. The variables for the ego vehicle, surrounding vehicles, and driving environment used in the sample scenario are expressed in Table 1. Fig. 8(a) illustrates the single vehicle risk based on obstacle vehicle O_1,

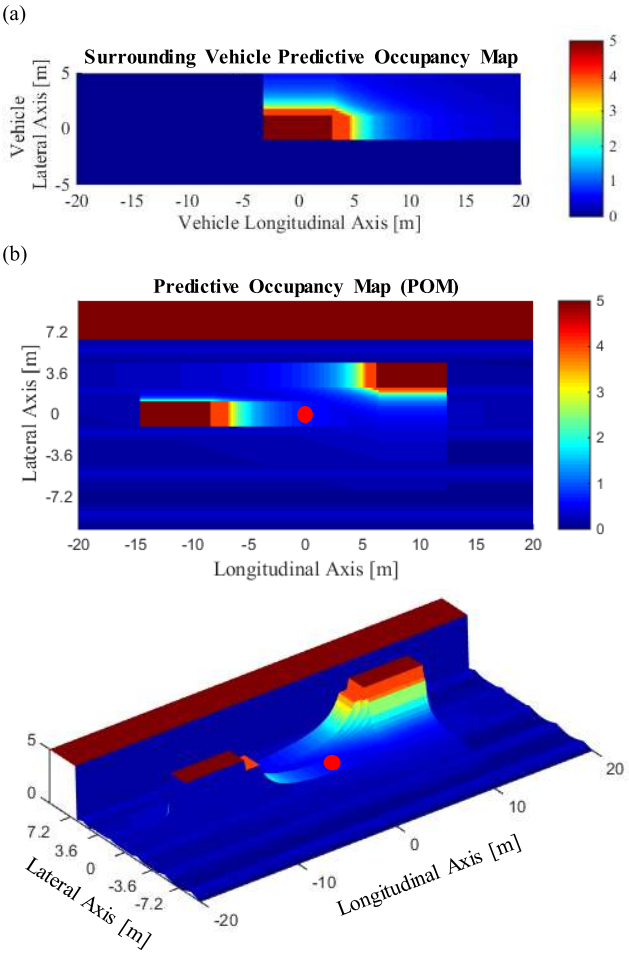

FIGURE 8. Concept of predictive occupancy map (POM) with sample scenario (a) Obstacle vehicle O_1 risk, (b) Predictive occupancy map with x-y axis view, and x-y-z view.

TABLE 1. Vehicle and driving environment sample scenario.

	Parameter		Value		
			Ego	O1	O2
Vehicle	Position (x)	p_x (m)	0	-12	10
	Position (y)	p_y (m)	0	0	3.6
	Velocity (x)	V_x (m/s)	22.2	27.8	16.7
	Velocity (y)	V_y (m/s)	0	0	-1.5
	Acceleration (x)	a_x (m/s^2)	0	0	0
	Acceleration (y)	a_y (m/s^2)	0	2	0
Driving Environment	Lane width	$lane_w$ (m)		3.6	
	Lane risk	$lane_r$		1/3	
	Left bound	B_l (m)		6.8	
	Right bound	B_r (m)		10	

while Fig. 8(b) illustrates the POM for surrounding vehicles O_1 and O_2 relative to the ego vehicle.

IV. MOTION PLANNING FOR COLLISION AVOIDANCE/MITIGATION

In this section, the safest route is selected based on the POM designed in the previous section. By utilizing the driving information from the ego vehicle, the maximum acceleration

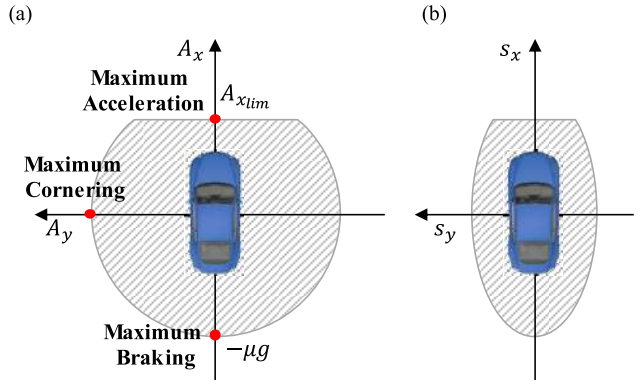

FIGURE 9. Ego vehicle acceleration limit and reachable region limit (a) Vehicle acceleration limit, (b) Reachable region limit under acceleration limit.

is calculated. Then, the reachable region limit, which is the maximum distance that can be reached within a limited time, is obtained. The drivable trajectories based on calculated reachable region limit are generated, and the risk of each trajectory is determined through the POM. The trajectory with the lowest risk value is selected and the longitudinal and lateral acceleration is calculated.

A. REACHABLE REGION

For stable operation of vehicle, it is necessary to determine the stability limit. The vehicle generally cannot produce a force equal to or greater than the frictional force limits of the tires. If force exceeds this limit, slip will occur and result in unstable and even uncontrollable vehicle operation. For safe control, trajectory must be planned within the g-g diagram, which is the maximum acceleration reachable within the force limit [30]. In the case of forward acceleration, the limit is assigned based on engine limit. Acceleration limit is described as

$$(\mu g)^2 = A_{x_{lim}}^2 + A_{y_{lim}}^2 \tag{18}$$

$$A_{x_{lim}} = \begin{cases} A_{e_{lim}}, & (A_{e_{lim}} \leq \sqrt{(\mu g)^2 - A_{y_{lim}}^2}) \\ \sqrt{(\mu g)^2 - A_{y_{lim}}^2}, & (A_{e_{lim}} > \sqrt{(\mu g)^2 - A_{y_{lim}}^2}) \end{cases} \tag{19}$$

where μ is the road friction coefficient, g is the gravitational acceleration, A_{lim} is the acceleration limit, derived from friction limit, and $A_{e_{lim}}$ is the acceleration limit from engine power. Equations (18) and (19) are also graphically illustrated in Fig. 9(a).

Based on the time limit relative to the acceleration limit, reachable vehicle positions are indicated. In the case of lateral motion, it is imperative that lateral vehicle velocity be zero after reaching the desired position. Therefore, the lateral position limit is half of the longitudinal position limit. Reachable regions are expressed as

$$S_{x_{lim}} = \frac{1}{2} A_{x_{lim}} t_f^2 \tag{20}$$

$$S_{y_{lim}} = \frac{1}{4} A_{y_{lim}} t_f^2 \tag{21}$$

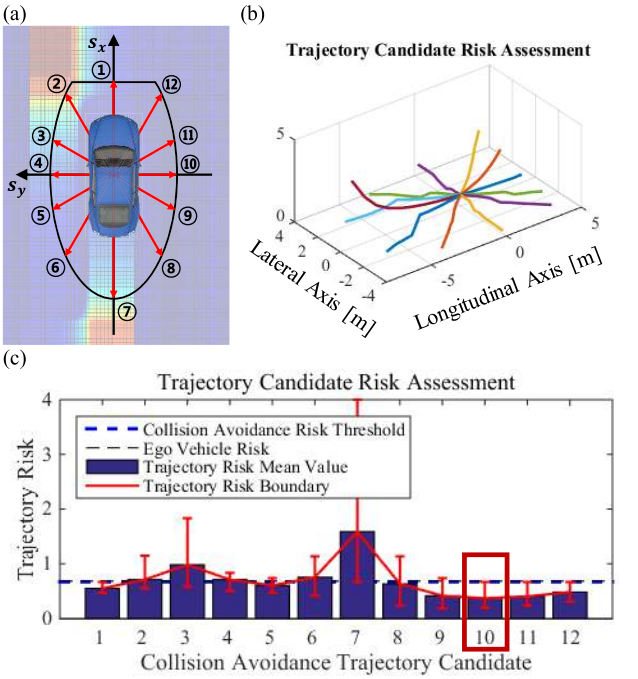

FIGURE 10. Trajectory candidate risk assessment with predictive occupancy map (POM), (a) Concept of trajectory candidate on POM, (b) Risk distribution of twelve trajectories, (c) Comparison of twelve trajectory candidates risk values with max, mean, and min values.

where S_{lim} is the reachable region limit within the CAMS active time under acceleration limit. Equations (20) and (21) are also graphically illustrated in Fig. 9 (b).

B. RISK ASSESSMENT OF TRAJECTORY CANDIDATES

Once a reachable region limit that guarantees the stability of the vehicle in time is determined, trajectory candidates can be set within the limit. A total of 12 pre-determined trajectories that are 30 degrees apart are assigned and are expressed as follows.

$$\begin{aligned} \text{Trajectory}_i &= \sqrt{S_{i_{x_{lim}}}^2 + S_{i_{y_{lim}}}^2} \\ \textit{for } i \in T\,[1, 2, \cdots, 12] &= T[0°, 30°, \cdots, 330°] \end{aligned} \tag{22}$$

Using the sum of risks from each trajectory until CAMS algorithm is completed, the 12 trajectories can be combined with the POM to indicate the risk of each trajectory. The trajectory generated based on the sample scenario coupled with POM is shown in Fig. 10 (a), while the risk values of each of the 12 routes are shown in Fig. 10 (b). There is a fast approaching obstacle vehicle O_1 at the rear of the ego vehicle, which generates a high risk. On the leftward route of the ego vehicle, the POM predicts that vehicle could collide with obstacle vehicle O_2, thus also generating a high risk at this trajectory. On the other hand, the rightward route of the vehicle shows low risk.

Within the 12 pre-determined trajectories, it is important to select the safest route through fair comparison. To select the safest route, 10 points of each route are selected because

each trajectory length is different, and the max, mean, and min values are calculated as

$$RA_{tra_i max} = \max\left\{\sum_{c=1}^{10} POM\left(\frac{c}{10}S_{i_x}, \frac{c}{10}S_{i_y}\right)\right\} \quad (23)$$

$$RA_{tra_i mean} = \text{mean}\left\{\sum_{c=1}^{10} POM\left(\frac{c}{10}S_{i_x}, \frac{c}{10}S_{i_y}\right)\right\} \quad (24)$$

$$RA_{tra_i min} = \min\left\{\sum_{c=1}^{10} POM\left(\frac{c}{10}S_{i_x}, \frac{c}{10}S_{i_y}\right)\right\} \quad (25)$$

Through Eq. (23)-(25), comparison of the 12 trajectories can be illustrated, as shown in Fig. 10(c). The blue bar of Fig. 10(c) represents the mean value of the trajectory candidate risk. The red bars are the boundary of trajectory risk with max and min values.

Conditions for safe trajectory are assigned as follows. The trajectory risk with a max value that does not exceed the threshold value ($Traj_{threshold}$) as

$$RA_{tra_i max} \leq Traj_{threshold} \quad (26)$$

After satisfying the first condition in Eq. (26), the trajectory risk with the lowest mean value is selected.

$$\text{Trajectory}_i = \underset{i \in T}{\text{argmin}}\ (RA_{tra_i mean}) \quad (27)$$

When multiple trajectories that satisfy the condition in Eq. (27) are present, the trajectory risk with the lowest min value is selected; this is ultimately the safest route for the vehicle.

$$\text{Trajectory}_i = \underset{i \in T}{\text{argmin}}\ (RA_{tra_i min}) \quad (28)$$

In the sample scenario based on Table 1, the safest trajectory that satisfied condition Eq. (26)-(28) is trajectory candidate number 10.

C. ACCELERATION PROFILE PLANNING

After selecting the safest trajectory from the previous subsection, acceleration planning is performed. The safest trajectory is selected while considering that vehicle is in motion. Therefore, the longitudinal and lateral acceleration and velocity are independently considered depending on direction of trajectory. The vehicle's acceleration is determined based on the final trajectory the vehicle selects. The x-axis and y-axis accelerations of the final trajectory are described as

$$A_x = 2S_x \cdot \frac{1}{t_f^2} \quad (29)$$

$$A_y = \begin{cases} 4S_y \cdot \dfrac{1}{t_f^2} & (0 \leq t_{CA} < \dfrac{1}{2}t_f) \\ -4S_y \cdot \dfrac{1}{t_f^2} & (\dfrac{1}{2}t_f \leq t_{CA} < t_f) \end{cases} \quad (30)$$

where (S_x, S_y) is the collision avoidance/mitigation final point when final time (t_f), and A_x, A_y are the accelerations, for reaching collision avoidance/mitigation final point.

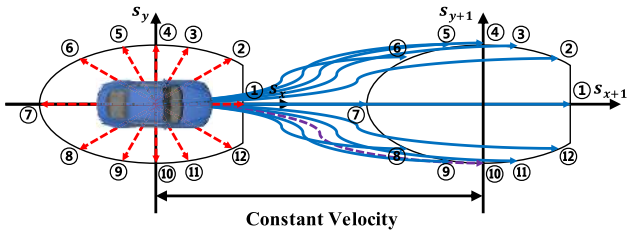

FIGURE 11. Each acceleration-based trajectory (red dash line) corresponds to global trajectory (blue solid line).

When planning acceleration trajectory based on a reachable region, the vehicle's movement path in global coordinates is shown in Fig. 11. Each red dash acceleration trajectory corresponds to a blue solid path after t_{CAMS} seconds. The trajectory candidate number 10 that selected at sample scenario is highlighted purple dash line at Fig. 11.

V. PERFORMANCE EVALUATIONS

In this section, a multi-vehicle collision scenario simulation was designed, and operation of proposed algorithm was verified.

A. SIMULATION SETTINGS

The risk threshold ($\text{Risk}_{\text{threshold}}$) and CAMS final time ($t_f$) are tuning parameters for when to turn on CAMS in a risky situation. In this simulation, reachable region limit (S_{lim}) is set to the distance of a change of one traffic lane (= 3.6 m) in a collision situation. The CAMS final time (t_f) is acquired with S_{lim} and μg through Eq. (21). The value t_f is expressed as

$$t_f = \sqrt{4 \cdot S_{y_{lim}} \cdot \frac{1}{\mu g}} \quad (31)$$

To safely escape during t_f seconds, the CAMS must be activated at least t_f seconds before the predicted collision. Therefore, the risk threshold is as follows

$$\text{Risk}_{\text{threshold}} = 1/t_f \quad (32)$$

The lane risk is a tuning parameter indicating the preference for longitudinal and lateral avoidance motion. The lane risk is 1/3, which is the condition for lateral avoidance only in a situation in which longitudinal avoidance in inevitable. The detailed simulation settings are expressed in Table 2.

B. COLLISION SCENARIOS FOR SIMULATION

The scenarios for simulation were designed for side collision and backward collision scenarios. The two scenarios are collision threat situations due to the carelessness of nearby vehicles, and are not caused by the ego vehicle. To simulate the multi-vehicle collision scenario, vehicles were placed in positions where it would be easy for the ego vehicle to maneuver to avoid collision.

In the scenario that considers side collision, vehicle from one side abruptly enters the lane where ego vehicle is located,

TABLE 2. Simulation settings.

		Parameter	Value
Ego vehicle	Vehicle limit	μg (m/s^2)	7.2
	Engine limit	$A_{e,lim}$ (m/s^2)	4
Collision Avoidance/Mitigation System	Risk threshold	$Risk_{threshold}$	0.7
	Trajectory threshold	$Traj_{threshold}$	2
	CAMS final time	t_f (s)	1.4
Driving Environment	Lane width	$lane_w$ (m)	3.6
	Lane risk	$lane_r$	1/3
	Left bound	B_l (m)	6.8
	Right bound	B_r (m)	10

and another vehicle is also present in the opposite lane. The ego vehicle is travelling at a velocity of 22.2m/s, and obstacle vehicles O_1 and O_2 in both opposing lanes are travelling at identical velocity. Obstacle vehicle O_1 is approaching the ego vehicle with a lateral velocity of 1.5m/s. Typically, the ego vehicle can avoid collision by changing to the opposing lane, away from O_1. However, in this special case, obstacle vehicle O_2 is present in the opposing lane. Therefore, the CAMS motion is observed another safe route.

In the second scenario, which considers backward collision, a vehicle located at the rear of the ego vehicle is approaching and it is also not decelerating. There have been many incidents where vehicles collide with a lead vehicle due to driver's drowsiness or negligence about surroundings. Similar to the first scenario, the ego vehicle is travelling at a velocity of 22.2m/s, and vehicle O_1, located 20m behind the ego vehicle, is approaching at a velocity of 33.3m/s. Also, vehicle O_2 is 20m in front of the ego vehicle, which is cruising at a velocity of 11.1m/s. This scenario has been designed to observe that vehicle with proposed algorithm can successfully detect fast approaching vehicle from the rear and avoid collision by changing lanes. Each scenario is illustrated in Fig. 12.

C. SIMULATION RESULTS

The simulation results for both 'side collision' and 'backward collision' are presented at Fig. 13 and Fig. 14, respectively. Figs. 13(a) and 14(a) illustrate the local position after CAMS has been turned on for 0 seconds, 0.5 seconds, 1.0 second, and 1.5 seconds. Figs. 13(b) and 14(b) show POM for each situation. Figs. 13(c) and 14(c) show graphs that compare the risk of each trajectory once CAMS is ON. Finally, Figs. 13(d) and 14(d) show the calculated lateral and longitudinal acceleration based on selected trajectory.

In first scenario result at the 0 second mark is shown in Fig. 13 (b); the right vehicle moves left, and risk of collision increases. As ego vehicle notices the danger of collision, it assesses the risk of 12 pre-determined trajectories as shown in Fig. 13(c), and selects trajectory 7, which has the lowest mean value. Trajectory 7 will only activate the brakes of the vehicle, and thus it can be observed that longitudinal acceleration decreases, as shown in Fig. 13(d). The vehicle

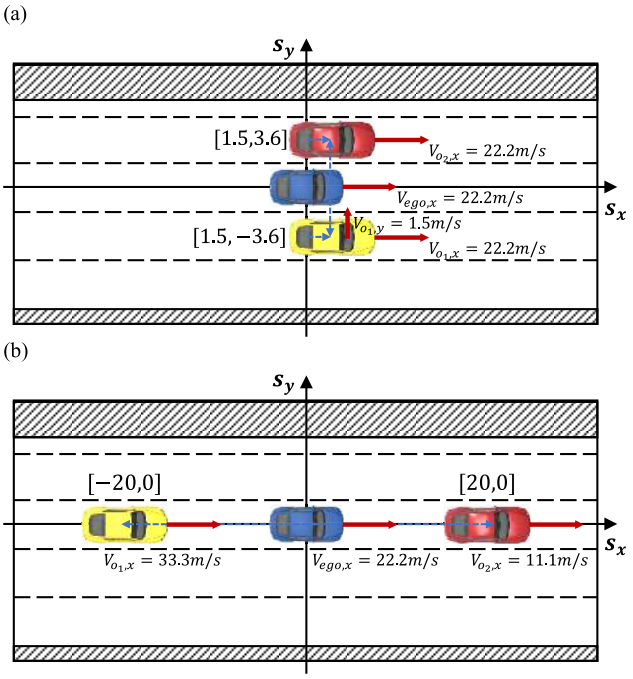

FIGURE 12. Collision simulation scenarios. (a) Side collision scenario, (b) backward collision scenario.

decelerated to 7.2m/s^2, and reduced velocity to 12.1m/s at 1.4 seconds, which is the time at which CAMS deactivated. When observing each state at 0.5 seconds, 1.0 second, and 1.5 seconds, as shown in Fig. 13(a), it can be verified that the vehicle successfully decelerated within the controllable limit and avoided the right-side vehicle approaching the lane.

At the 0 second mark of the second scenario, shown in Fig. 14(b), the POM for the front and rear positions of the ego vehicle generate high risk of collision. The twelve pre-determined trajectories are compared again, as shown in Fig. 14(c), and trajectories 4 and 10, with the lowest mean values, are selected. In this case, trajectory 10 is randomly selected because of the mean values of risk of trajectories 4 and 10 are the same. Trajectory 10 maintains the ego vehicle's velocity while increasing the lateral acceleration towards the right, as illustrated in Fig. 14(d). It can be observed that maximum lateral acceleration to one side is generated, and then lateral acceleration of the opposite side is generated once reaching the halfway point. The vehicle generated a maximum lateral velocity of 5.0m/s while moving 3.6m to the right and reached lateral velocity of 0 m/s at 1.4 seconds, which is when CAMS deactivated. As ego vehicle avoided collision, it can be observed that obstacle vehicle O_1 and O_2 have collided. While this is not an ideal case, it shows a worst-case scenario. When a similar situation occurs in the real-world environment, the vehicle located at the rear will have enough time to react with the ego vehicle out of the way, and thus collision will be avoided.

Through the two scenarios, the operation of the proposed algorithm has been verified. By assessing collision risks

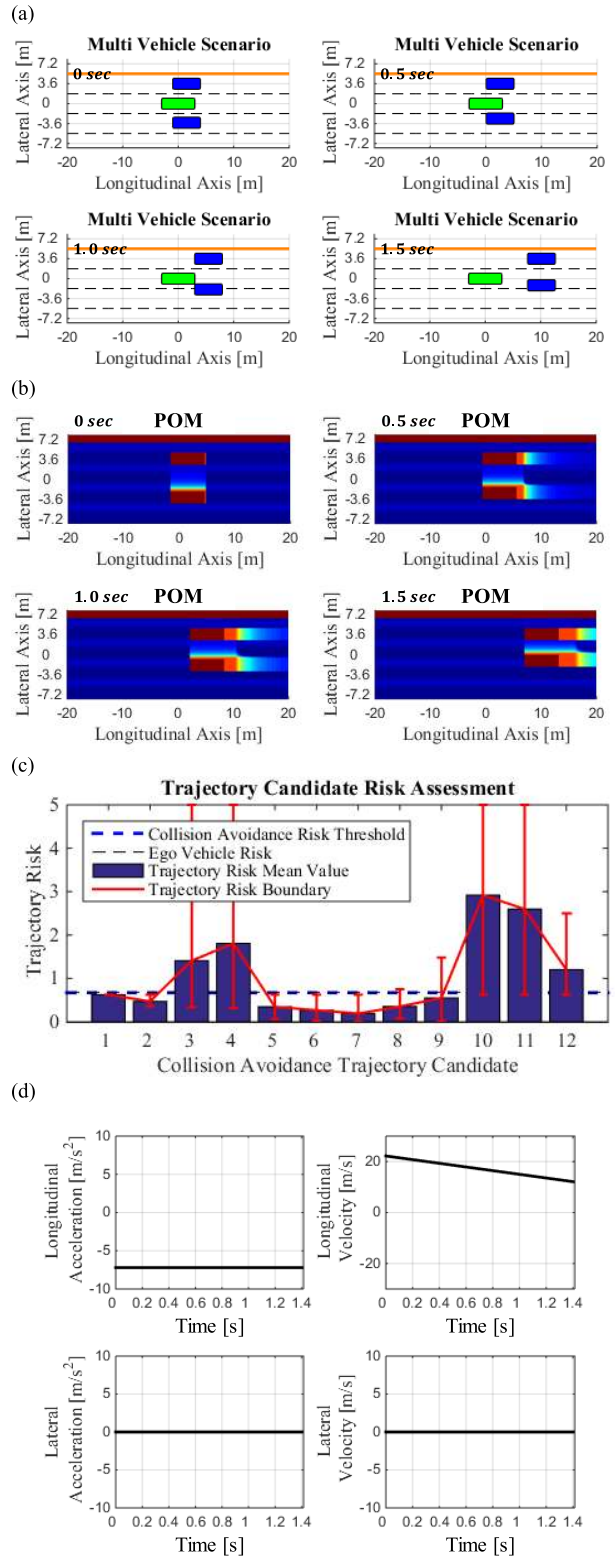

FIGURE 13. Simulation results of side collision scenario. (a) Time series vehicle position (0sec, 0.5sec, 1.0sec, 1.5sec), (b) POM of each time (0sec, 0.5sec, 1.0sec, 1.5sec), (c) Comparison of trajectory candidate risk when CAMS starts, (d) Planned longitudinal and lateral acceleration profile when CAMS starts.

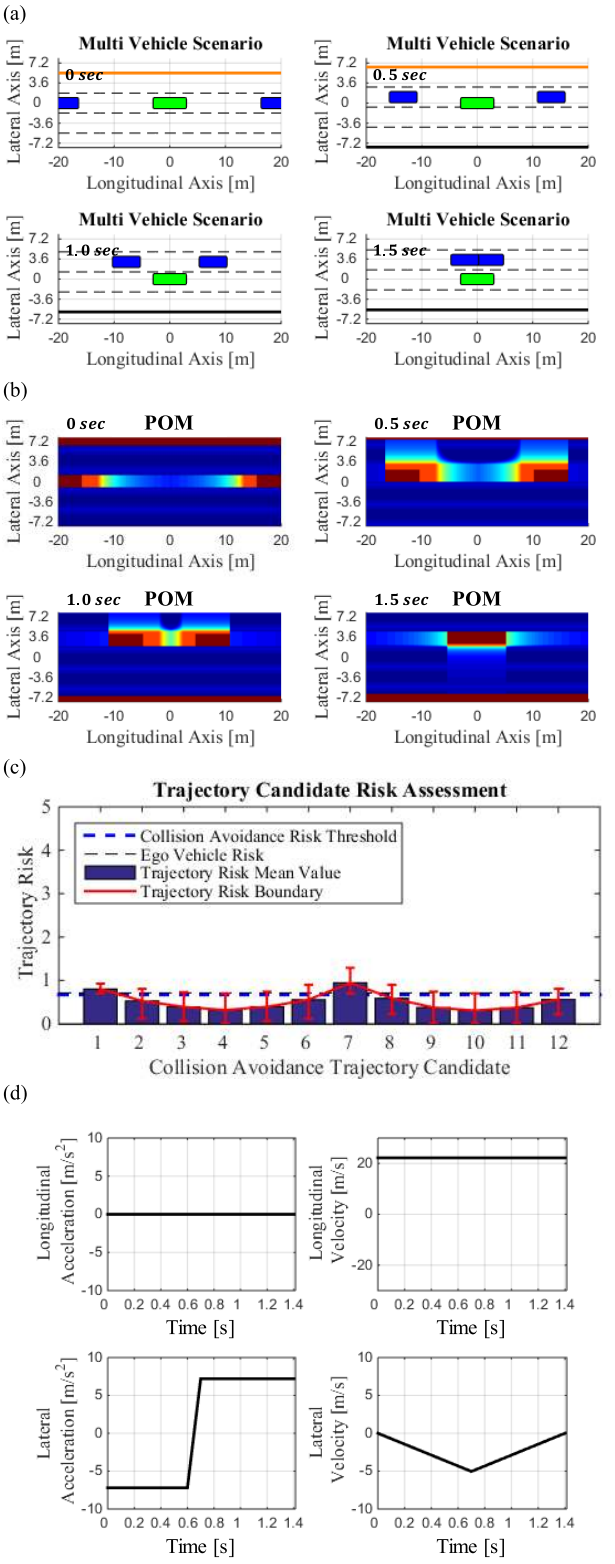

FIGURE 14. Simulation results of backward collision scenario. (a) time series vehicle position (0sec, 0.5sec, 1.0sec, 1.5sec), (b) POM of each time (0sec, 0.5sec, 1.0sec, 1.5sec), (c) Comparison of trajectory candidate risk when CAMS starts, (d) Planned longitudinal and lateral acceleration profile when CAMS starts.

within the vehicle' surroundings and generating a time-dependent map, the vehicle was able to perform evasive maneuvers and avoid collision within the 1.4 second time frame. Furthermore, the proposed algorithm generates its trajectory by calculating acceleration based on the sensors equipped on the ego vehicle. Thus, it can successfully generate avoidance trajectories without relying on global coordinate way points provided through localization map or accurate GPS.

VI. CONCLUSION

This paper proposes a novel algorithm that determines potential risks based another vehicle's sudden unexpected maneuver; it does not focus only on the ego vehicle. To observe future potential risks of collision, a POM has been developed that identifies the surroundings in spatial and temporal space. Through the POM, potential risks of collision with multiple vehicles can be determined simultaneously, and risk affiliated with each position based on time can be identified, allowing intuitive identification of the safest space for the ego vehicle. Through the POM, the safest avoidance trajectory can be selected after analytically comparing multiple trajectory candidates. The surrounding trajectory candidates were generated based on vehicle acceleration limit, which allowed simultaneous planning of the trajectory and velocity profile. The operation feasibility of the proposed algorithm was verified through two simulation scenarios as the ego vehicle successfully avoided a potential collision.

Through this study, the safety of autonomous vehicles can be further improved by providing an avoidance trajectory focused on surrounding vehicles, rather than focusing on the ego vehicle itself. The current scenarios used in the simulation have only focused on straight roads, and will be evaluated for curved roads in future research.

REFERENCES

[1] D. Sam, C. Velanganni, and T. E. Evangelin, "A vehicle control system using a time synchronized hybrid VANET to reduce road accidents caused by human error," *Veh. Commun.*, vol. 6, pp. 17–28, Oct. 2016.
[2] F. M. Favarò, N. Nader, S. O. Eurich, M. Tripp, and N. Varadaraju, "Examining accident reports involving autonomous vehicles in California," *PLoS ONE*, vol. 12, no. 9, 2017, Art. no. e0184952.
[3] F. Favarò, S. Eurich, and N. Nader, "Autonomous vehicles' disengagements: Trends, triggers, and regulatory limitations," *Accident Anal. Prevention*, vol. 110, pp. 136–148, Jan. 2018.
[4] Y. Zhang *et al.*, "Hybrid trajectory planning for autonomous driving in highly constrained environments," *IEEE Access*, vol. 6, pp. 32800–32819, 2018.
[5] J. Guo, P. Hu, and R. Wang, "Nonlinear coordinated steering and braking control of vision-based autonomous vehicles in emergency obstacle avoidance," *IEEE Trans. Intell. Transp. Syst.*, vol. 17, no. 11, pp. 3230–3240, Nov. 2016.
[6] R. Isermann, M. Schorn, and U. Stählin, "Anticollision system PRORETA with automatic braking and steering," *Vehicle Syst. Dyn.*, vol. 46, no. 1, pp. 683–694, 2008.
[7] T. Hesse and T. Sattel, "An approach to integrate vehicle dynamics in motion planning for advanced driver assistance systems," in *Proc. IEEE Intell. Vehicle Symp. (IV)*, Jun. 2007, pp. 1240–1245.
[8] C. Guo, K. Kidono, T. Machida, R. Terashima, and Y. Kojima, "Human-like behavior generation for intelligent vehicles in urban environment based on a hybrid potential map," in *Proc. IEEE Intell. Vehicle Symp. (IV)*, Jun. 2017, pp. 197–203.
[9] F. Bounini, D. Gingras, H. Pollart, and D. Gruyer, "Modified artificial potential field method for online path planning applications," in *Proc. IEEE Intell. Vehicle Symp. (IV)*, Jun. 2017, pp. 180–185.
[10] J. Ji, A. Khajepour, W. W. Melek, and Y. Huang, "Path planning and tracking for vehicle collision avoidance based on model predictive control with multiconstraints," *IEEE Trans. Veh. Technol.*, vol. 66, no. 2, pp. 952–964, Feb. 2017.
[11] Y. Rasekhipour, A. Khajepour, S.-K. Chen, and B. Litkouhi, "A potential field-based model predictive path-planning controller for autonomous road vehicles," *IEEE Trans. Intell. Transp. Syst.*, vol. 18, no. 5, pp. 1255–1267, May 2017.
[12] R. Bis, H. Peng, and G. Ulsoy, "Velocity occupancy space: Robot navigation and moving obstacle avoidance with sensor uncertainty," in *Proc. ASME Dyn. Syst. Control Conf.*, 2009, pp. 363–370.
[13] K. Kim, K. Lee, B. Ko, and K. Yi, "Design of integrated risk management-based dynamic driving control of automated vehicles," *IEEE Intell. Transp. Syst. Mag.*, vol. 9, no. 1, pp. 57–73, Jan. 2017.
[14] S. Yoon and D. Kum, "The multilayer perceptron approach to lateral motion prediction of surrounding vehicles for autonomous vehicles," in *Proc. IEEE Intell. Vehicle Symp. (IV)*, Jun. 2016, pp. 1307–1312.
[15] B. Kim *et al.* (Sep. 2017). "Probabilistic vehicle trajectory prediction over occupancy grid map via recurrent neural network." [Online]. Available: https://arxiv.org/abs/1704.07049
[16] H.-S. Jeon, D.-S. Kum, and W.-Y. Jeong, "Traffic scene prediction via deep learning: Introduction of multi-channel occupancy grid map as a scene representation," in *Proc. IEEE Intell. Vehicle Symp. (IV)*, Jun. 2018, pp. 1496–1501.
[17] S. Lefèvre, D. Vasquez, and C. Laugier, "A survey on motion prediction and risk assessment for intelligent vehicles," *ROBOMECH J.*, vol. 1, no. 1, pp. 1–14, 2014.
[18] J. Hillenbrand, A. M. Spieker, and K. Kroschel, "A multilevel collision mitigation approach—Its situation assessment, decision making, and performance tradeoffs," *IEEE Trans. Intell. Transp. Syst.*, vol. 7, no. 4, pp. 528–540, Dec. 2006.
[19] A. Polychronopoulos, M. Tsogas, A. J. Amditis, and L. Andreone, "Sensor fusion for predicting vehicles' path for collision avoidance systems," *IEEE Trans. Intell. Transp. Syst.*, vol. 8, no. 3, pp. 549–562, Sep. 2007.
[20] M. Schreier, V. Willert, and J. Adamy, "An integrated approach to maneuver-based trajectory prediction and criticality assessment in arbitrary road environments," *IEEE Trans. Intell. Transp. Syst.*, vol. 17, no. 10, pp. 2751–2766, Oct. 2016.
[21] A. Broadhurst, S. Baker, and T. Kanade, "Monte Carlo road safety reasoning," in *Proc. IEEE Intell. Vehicle Symp. (IV)*, Jun. 2005, pp. 319–324.
[22] R. Chen, R. Sherony, and H. C. Gabler, "Comparison of time to collision and enhanced time to collision at brake application during normal driving," SAE Tech. Paper 2016-01-1448, 2016.
[23] A. Berthelot, A. Tamke, T. Dang, and G. Breuel, "A novel approach for the probabilistic computation of time-to-collision," in *Proc. IEEE Intell. Vehicle Symp.*, Jun. 2012, pp. 1173–1178.
[24] I. B. Yang, S. G. Na, and H. Heo, "Intelligent algorithm based on support vector data description for automotive collision avoidance system," *Int. J. Automot. Technol.*, vol. 18, no. 1, pp. 69–77, 2017.
[25] G. R. de Campos, A. H. Runarsson, F. Granum, P. Falcone, and K. Alenljung, "Collision avoidance at intersections: A probabilistic threat-assessment and decision-making system for safety interventions," in *Proc. 17th IEEE Int. Conf. Intell. Transp. Syst.*, Oct. 2014, pp. 649–654.
[26] B. Kim and K. Yi, "Probabilistic and holistic prediction of vehicle states using sensor fusion for application to integrated vehicle safety systems," *IEEE Trans. Intell. Transp. Syst.*, vol. 15, no. 5, pp. 2178–2190, May 2014.
[27] C. Laugier *et al.*, "Probabilistic analysis of dynamic scenes and collision risks assessment to improve driving safety," *IEEE Intell. Transp. Syst. Mag.*, vol. 3, no. 4, pp. 4–19, Oct. 2011.
[28] J. Kim and D. Kum, "Collision risk assessment algorithm via lane-based probabilistic motion prediction of surrounding vehicles," *IEEE Trans. Intell. Transp. Syst.*, vol. 19, no. 9, pp. 2965–2976, Sep. 2018.
[29] X. Wang, M. Chen, M. Zhu, and P. Tremont, "Development of a kinematic-based forward collision warning algorithm using an advanced driving simulator," *IEEE Trans. Intell. Transp. Syst.*, vol. 17, no. 9, pp. 2583–2591, Sep. 2016.
[30] W. F. Milliken and D. L. Milliken, *Race Car Vehicle Dynamics*. Pittsburgh, PA, USA: SAE International, 1995, pp. 345–359.

KIBEOM LEE received the master's degree from the Korea Advanced Institute of Science and Technology (KAIST), Daejeon, South Korea, in 2014, where he is currently pursuing the Ph.D. degree. His research interests include the fields of vehicle dynamics, advanced driver assist systems, control, and autonomous vehicles.

DONGSUK KUM received the Ph.D. degree in mechanical engineering from the University of Michigan, Ann Arbor, MI, USA, in 2010.

He was with the General Motors R&D Propulsion Systems Research Laboratory, Warren, MI, USA, as a Visiting Research Scientist. His works at General Motors focused on advanced propulsion system technologies, including hybrid electric vehicles, flywheel hybrid, and waste heat recovery systems. He is currently an Assistant Professor with the Graduate School for Green Transportation, Korea Advanced Institute of Science and Technology (KAIST), and the Director of the Vehicular System Design and Control (VDC) Laboratory. His research interests include the modeling, control, and design of advanced vehicular systems with particular interests in hybrid electric vehicles and autonomous vehicles